Review article

Xuexin Ren, Pankaj K. Jha, Yuan Wang and Xiang Zhang*

Nonconventional metasurfaces: from non-Hermitian coupling, quantum interactions, to skin cloak

Abstract: Metasurfaces are optically thin layers of sub-
wavelength resonators that locally tailor the electromag-
netic response at the nanoscale. Our metasurface research
aims at developing novel designs and applications of
metasurfaces that go beyond the classical regimes. In con-
trast to conventional phase gradient metasurfaces where
each meta-atom responds individually, we are interested
in developing metasurfaces where neighboring meta-
atoms are strongly coupled. By engineering a non-Her-
mitian coupling between the meta-atoms, new degrees
of freedom are introduced and novel functionalities can
be achieved. We are also interested in combining classi-
cal metasurface with quantum emitters, which may offer
opportunities for on-chip quantum technologies. Addi-
tionally, we have been designing metasurfaces to realize
exciting phenomena and applications, such as ultrathin
metasurface cloak and strong photonic spin-Hall effect. In
this paper, we review our research efforts in optical meta-
surfaces in the past few years, which ranges from conven-
tional to novel type of metasurface and from classical to
quantum regime.

---

*Corresponding author: Xiang Zhang, NSF Nanoscale Science and
Engineering Center (NSEC), University of California, 3112 Etcheverry
Hall, Berkeley, CA 94720, USA; and Materials Sciences Division,
Lawrence Berkeley National Laboratory, 1 Cyclotron Road, Berkeley,
CA 94720, USA, e-mail: xiang@berkeley.edu
Xuexin Ren and Pankaj K. Jha: NSF Nanoscale Science and
Engineering Center (NSEC), University of California, 3112 Etcheverry
Hall, Berkeley, CA 94720, USA
Yuan Wang: NSF Nanoscale Science and Engineering Center (NSEC),
University of California, 3112 Etcheverry Hall, Berkeley, CA 94720,
USA; and Materials Sciences Division, Lawrence Berkeley National
Laboratory, 1 Cyclotron Road, Berkeley, CA 94720, USA

1 Introduction

Metamaterials are artificial materials that consist of sub-
wavelength unit cells (meta-atoms). They attain their
electromagnetic properties from the unit cell response
rather than the constituent materials and can be designed
to exhibit properties that are not readily found in natural
materials. Since Pendry et al.'s proposal of using metal-
lic wires [1] and split-ring resonators [2] to realize negative
permittivity and negative permeability [3], respectively,
metamaterials have gained monumental research inter-
ests. The study of metamaterials has opened up a route
to many exciting applications, such as superresolution
imaging [4, 5] and invisibility cloaks [6]. Unfortunately,
despite huge research effort and significant accomplish-
ments, these potential applications are still hindered
in practice by the significant absorptive loss in metallic
structures as well as the difficulty in the fabrication of 3D
structures.

In recent years, a significant amount of research
effort has shifted to the study of metasurfaces, which can
be considered as 2D metamaterials. Due to their reduced
dimensionality, metasurfaces are much easier to fabri-
cate and yet offer a higher degree of freedom in molding
the flow of waves (optical, acoustic) compared to bulk
metamaterials. Being optically thin, metasurfaces have
reduced absorptive loss and thus offer higher efficiency.
Metasurfaces use resonances to achieve abrupt phase
shift on subwavelength-scale distances [7–10] in contrast
to traditional optical devices that rely on propagation
effect. By carefully designing each meta-atom to locally
control the phase shift, the so-called phase gradient meta-
surface can tailor wavefronts at will. Typical examples of
meta-atoms include multiresonance antennas [11, 12],
gap-plasmon resonators [13], Pancharatnam-Berry-phase
structures [14], and Huygen's atoms [15]. The outstanding
optical performance and design flexibility of phase gradi-
ent metasurface have led to the development of various
planar optical devices, such as metasurface planar lens

[16, 17], metaholograms [18, 19], and multifunctional metasurfaces [20].

Our group is interested in developing metasurfaces with unique physics that enable novel functionalities. Based on the design principle of phase gradient metasurface, we have experimentally realized exciting phenomena and functionalities, including strong photonic spin-Hall effect (PSHE) [21] and ultrathin invisibility skin cloak at visible wavelength [22]. Furthermore, we are interested in combining classical phase gradient metasurfaces with quantum emitters, which may open up opportunities for on-chip quantum state engineering. By placing a judiciously designed metasurface at the far field of quantum emitters, we theoretically showed that phenomena such as quantum interference between orthogonal decay channels [23] and qubit entanglement [24] could be achieved.

Classical phase gradient metasurfaces work in the regime where the meta-atoms need to be well separated such that the interaction between neighboring meta-atoms is negligible. Consequently, each meta-atom can be treated independently and the functionality of the whole metasurface is derived from individual meta-atoms. Our group is interested in developing a novel type of metasurfaces, where the neighboring meta-atoms can be strongly coupled and the coupling efficiencies are uniquely engineered. Specifically, we demonstrated that, by tailoring the couplings to be anti-Hermitian, the spatial manipulation of light at the deep subwavelength scales could be realized [25]. We expect that, by introducing coupling as a new degree of freedom in the metasurface design, more novel properties can be achieved. In this paper, we review our research in optical metasurface in the past few years, including anti-Hermitian coupled meta-atoms, PSHE at metasurfaces, ultrathin invisibility skin cloak, as well as quantum interference with metasurfaces.

2 Anti-Hermitian coupled meta-atoms

Meta-atoms can be viewed as quasi-bound states, which interact with each other via direct near-field coupling as well as indirect coupling mediated by radiative channels. Indirect couplings in quasi-bound states have been widely studied in various open quantum systems, including nuclei, atoms, molecules, and quantum dots [26]. It has been shown that the indirect coupling gives rise to an imaginary or anti-Hermitian coupling matrix in the system. The original and unperturbed eigenstates in the system hybridize to form new eigenstates, and due to the anti-Hermitian coupling, some of the new eigenstates are decoupled from the decay channels and have very long lifetimes, whereas others have enhanced decay rates and can radiate very strongly (superradiant state).

In plasmonic systems, anti-Hermitian couplings have played an important role in introducing interference among different excitation pathways. Aside from the well-studied plasmon-induced transparency [27, 28] and interacting dark resonance [29], which comes from destructive interference between isolated and continuum states, opposite phenomena such as electromagnetically induced absorption and superscattering have also been demonstrated. In 2012, our group showed that the anti-Hermitian coupling could also be used to spatially manipulate light at the deep subwavelength scale [25]. We showed that, by designing an anti-Hermitian coupling matrix, a system of plasmonic meta-atoms closely packed within only $\lambda/15$ separations can be individually excited from the far field, which are otherwise indistinguishable from each other.

We begin with a system that consists of two closely spaced plasmonic antennas, where the resonant wavelength of each antenna is slightly different (Figure 1A). Due to the strong coupling between the antennas, the eigenstates of the system become hybridized excitations of two resonators. Therefore, in general, under plane wave excitation, both antennas will be excited. However, we found that, when the coupling is purely imaginary (anti-Hermitian), two simultaneously excited eigenstates interfere constructively at one resonator and destructively at the other, leading to a highly localized state. Although the coupling coefficient is generally a complex number, anti-Hermitian coupling coefficient can be achieved by carefully choosing the antenna separation, such that the real part from the direct and indirect couplings exactly cancel each other (Figure 1B).

In our experiment, we extended the system from two optical antennas to five optical antennas with deep subwavelength spacing (Figure 2). We theoretically showed that when the coupling constants between each pair of antennas were close to anti-Hermitian, highly localized states similar to the above could be achieved. We numerically retrieved the coupling constants and selected the separations so that the couplings were dominated by their anti-Hermitian part. Both simulations and near-field scattering optical measurements showed that each antenna could be individually excited at their resonance wavelength. We also fabricated a control sample where the
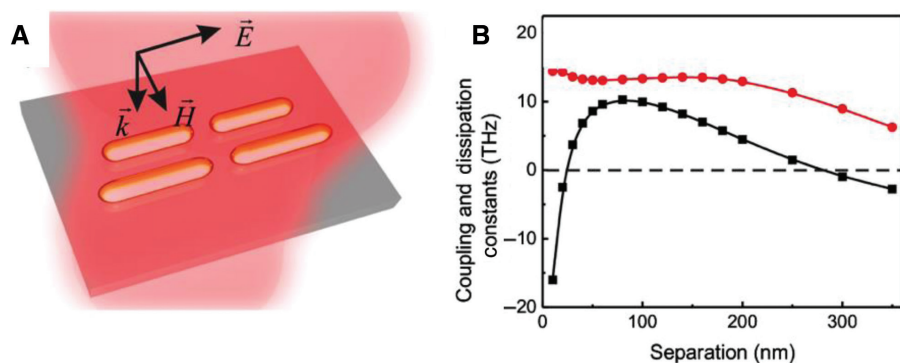
Figure 1: Optical coupling between two optical antennas, which include real (Hermitian) and imaginary (anti-Hermitian) couplings. (A) Plasmonic system consisting of two optical antennas made of gold. The system is deep subwavelength. (B) Simulated real part (black square) and imaginary part (red circle) of optical coupling constant between the two antennas, as a function of their separation s. The coupling consists both the direct near-field coupling and indirect coupling through the radiation channel. At a very small separation, the coupling has a huge negative real part that comes from the direct near-field coupling. When the spacing increases, the magnitude of the near-field coupling decreases rapidly. When s reaches 30 nm, the direct near-field coupling cancels with the real part from indirect far-field coupling, leaving a pure imaginary (anti-Hermitian) coupling. Reprinted from Ref. [25]. Copyright © 2012 by the American Physical Society.
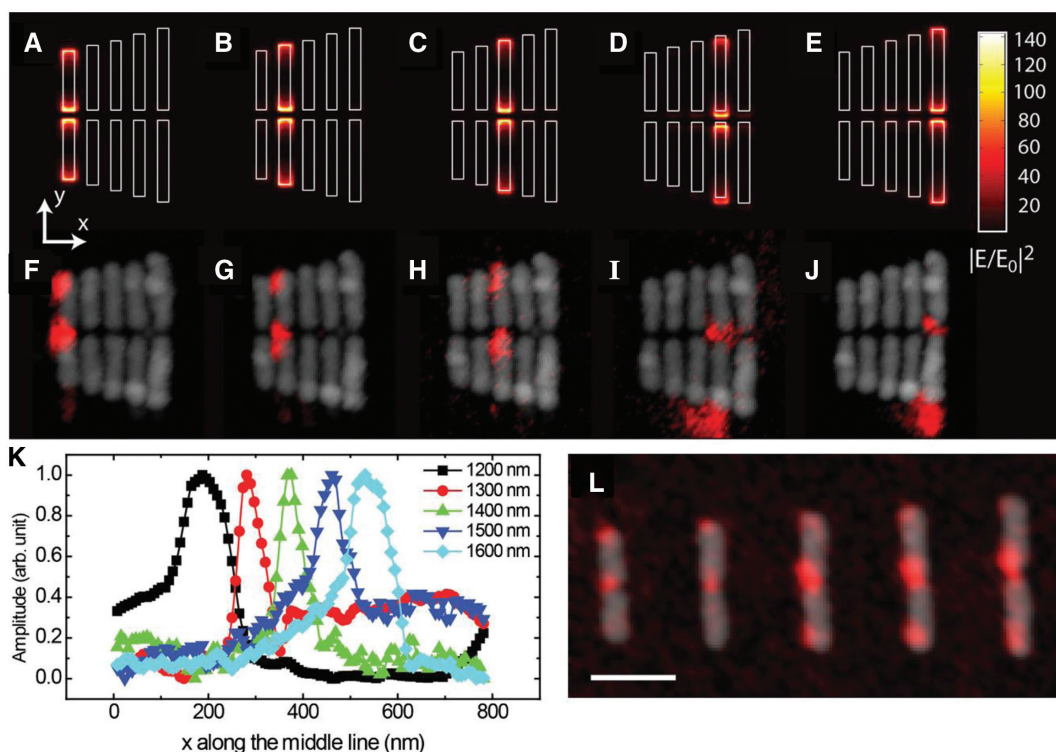

Figure 2: Experimental verification of the selective excitation of individual antennas in the plasmonic antenna array. (A–E) Simulated near-field distributions of the antenna array at five different wavelengths: 1200 nm (250 THz), 1300 nm (230.8 THz), 1400 nm (214.3 THz), 1500 nm (200 THz), and 1600 nm (187.5 THz). (F–J) Corresponding experimental observations show very good agreement with the simulations. (K) Measured intensity of light integrated along the y-direction, versus the x-direction, at each measured wavelength. (L) Near-field measurement at 1400 nm wavelength on the control sample, which consists of an array of antennas with the same geometry specification but at a large nearest neighbor separation of 300 nm. Reprinted from Ref. [25]. Copyright © 2012 by the American Physical Society.

separations between the antennas were much larger. In this case, no selective excitation was observed and all the antennas were excited simultaneously.

We believe that the anti-Hermitian coupling can open up a route for light manipulation at deep subwavelength scale and can introduce a new degree of freedom to

designing metasurfaces. We expect that it may also play an important role in high spatial resolution sensing due to its ability to eliminate detrimental crosstalk between neighboring resonators.

3 PSHE at metasurfaces

When meta-atoms are arranged on a surface, spatially varying phase shift can be engineered at will and novel device functionalities can be achieved. For example, meta-surfaces can be an important tool to control and study the spin-orbit coupling of light. We know from relativistic physics that particles can have interaction between its spin and its motion (i.e. spin-orbit coupling). Spin-orbit coupling has been observed in several particles, such as electrons, protons, and neutrons, and is the origin of many important phenomena, including the fine structure splitting in atom's energy levels [30] and magnetocrystalline anisotropy [31].

Photon possesses spin as well and theoretically should also exhibit spin-orbit coupling [32]. However, this coupling is usually very weak for photons and the amount of splitting can only be detected by performing quantum weak measurements with preselection and postselection of spin states [33]. In 2013, our group experimentally demonstrated strong spin-orbit interaction of light in a metasurface that contained spatially varying V-shaped nanoantennas [21]. We observed the PSHE, where light showed a transverse splitting in polarizations when light was refracted off the metasurface. The PSHE arises from the fact that the momentum and polarization of light are always perpendicular to each other (Figure 3). When light is propagating along a curved trajectory, the polarization of the light has to rotate accordingly to maintain the transverse property. As a back-action from geometric polarization rotations, the spin-orbit interaction also changes the propagation path of light, resulting in a helicity-dependent transverse displacement of light (i.e. PSHE). For an ordinary interface between two homogeneous media, when a Gaussian beam impinges onto the interface at normal incidence, the axial symmetry normal to the surface eliminates the spin-orbit coupling, and the total angular momentum of the entire beam is conserved. In our experiment, we designed a metasurface that introduced a rapid gradient of phase discontinuity along the interface, which broke the axial symmetry of the interface and allowed us to observe the PSHE.

The PSHE manifested by the metasurface can be directly measured with a camera by recording the polarization-dependent transport (Figure 4). Incident light with opposite helicity are both anomalously refracted at
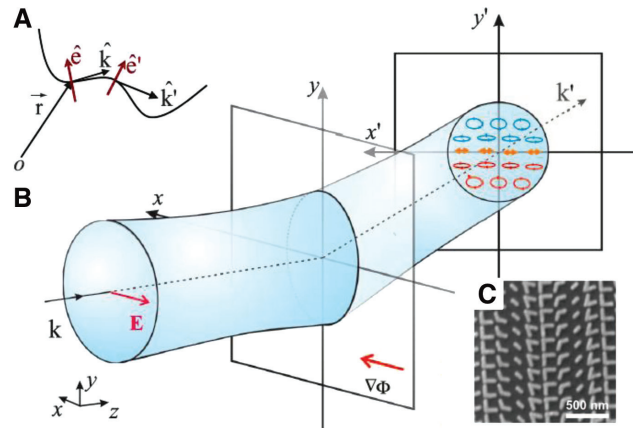
Figure 3: Giant photonic spin hall effect with metasurfaces. (A) Schematic of the PSHE. When light is propagating along a curved trajectory, the polarization of light will rotate accordingly. This is due to the transverse nature of light. (B) PSHE induced by a metasurface with a strong phase gradient along the x-direction. When the light beam is incident onto the metasurface, opposite circular components of the beam accumulate on the opposite side in the transverse directions. (C) Scanning electron microscopy (SEM) image of the fabricated metasurface. Reprinted from Ref. [21]. Copyright © 2013 by the AAAS.

the same angle but transversely transported against each other. We envision that the use of metasurface will open a new degree of freedom to control the flow of light and enable spin polarization-dependent novel functionalities.

4 Ultrathin metasurface invisibility skin cloak

Metamaterials have been used to realize invisibility cloaks, which can render objects to appear invisible to incoming waves. The design principle of metamaterial cloaking falls into two categories: scattering cancellation [34, 35] and transformation optics [6, 36, 37]. Scattering cancellation aims at cancelling out the major scattering field from an object and can be achieved using one or a few layers of plasmonic materials. This technique is mostly suitable for cloaking objects that are smaller than a few wavelengths, which have a small number of dominant scattering harmonics. The other method (transformation optics) manipulates the flow of electromagnetic energy using a transformation that stretches and compresses the Cartesian space. Because the Maxwell's equations have the same form under coordinate transformation, the wave propagation in the transformed space can be interpreted as propagation in the physical space that has a spatial distribution of permittivity ε and permeability μ.
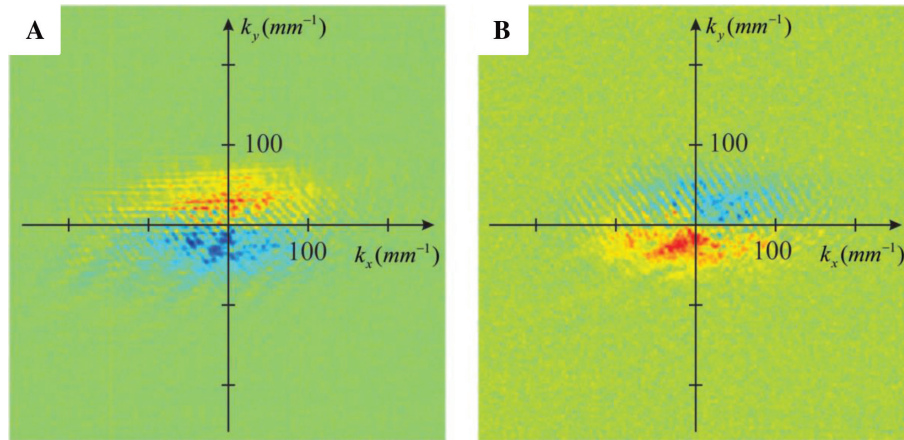
Figure 4: Characterization of spin hall effect.
(A) Observation of a giant SHE: the helicity of the anomalously refracted beam. The incidence light is polarized along the *x*-direction along the phase gradient of the metasurface. The incidence angle is at surface normal. Red and blue represent the right and left circular polarizations, respectively. (B) Helicity of the refracted beam with incidence polarized along the *y*-direction. Reprinted from Ref. [21]. Copyright © 2013 by the AAAS.

By specifically engineering ε and μ, metamaterials are therefore capable of controlling the trajectory of light that propagates inside. Since transformation cloaks were first proposed by Pendry et al. [36] and Leonhardt [37] in 2006, the concept was realized not only for electromagnetic waves but also extended to acoustic waves [38] and even the matter waves [39].

Transformation cloaks usually require extreme electromagnetic properties that are only achievable with metallic metamaterials and have been experimentally demonstrated in microwave frequencies [6]. The realization of such cloaks at optical frequencies is hindered by a significant optical (ohmic) loss. In 2008, Li and Pendry [40] proposed to use quasi-conformal mapping in transformation optics, which can reduce the requirement for extreme refractive index and anisotropy, allowing the use of dielectric metamaterials. This method laid the foundation of carpet cloaks, where the objects are hidden under a reflective layer (the carpet). Carpet cloak in visible range has later been experimentally demonstrated from microwave [41] to optical frequencies [42].

There are a few drawbacks of carpet cloaks, which hinder their applications in practice. First at all, carpet cloaks are typically very bulky. This is because they require a large volume for refractive index modulation to avoid extreme electromagnetic properties. As a result, complex 3D fabrication with very high spatial resolution is needed, and it is challenging to scale up this design to macroscopic objects. Moreover, in certain regions of the cloak, the varying index has to be smaller than the environment index, making it difficult to create a cloak that works in air. Consequently, the cloak is usually embedded in dielectrics of higher index, which introduces an additional phase shift in the reflected light and makes the optical cloak itself visible by phase-sensitive detection.

The recent development of metasurfaces provides another way to manipulate wave propagation. Metasurfaces are able to induce strong phase shift within a deep subwavelength distance, providing a route to very thin ($h \ll \lambda$) cloaks [43–45]. In 2015, our group experimentally demonstrated a metasurface-based invisibility skin cloak working at ~730 nm [22]. The cloak is an 80-nm-thick metasurface tightly wrapped over an object and can hide the object from optical detection (both intensity and phase detection). The metasurface skin cloak consists of subwavelength-scale gold nanoantennas, which can locally manipulate the phase of the reflected light over the 2π range, as shown in Figure 5. By specifically designing each nanoantennas, for any light incidence, the phase of the reflected light from the metasurface mimics that of light reflected from a flat mirror. As a result, the reflected light shows no scattering pattern from the object and the object disguises as a flat mirror. Moreover, because the phase is totally recovered, the object is undetectable even under phase-sensitive measurements.

With the complete wavefront and phase recovery from the metasurface skin cloak, we experimentally demonstrated concealing a 3D object of arbitrary for a specific light polarization. In our experiments, we fabricated an arbitrarily shaped 3D object with multiple bumps and dents, and the total size of the object is ~36×36 μm (Figure 6A and B). For each nanoantenna on the object, it compensated the phase difference between the light scattered from the object and that from the base plane. The metasurface
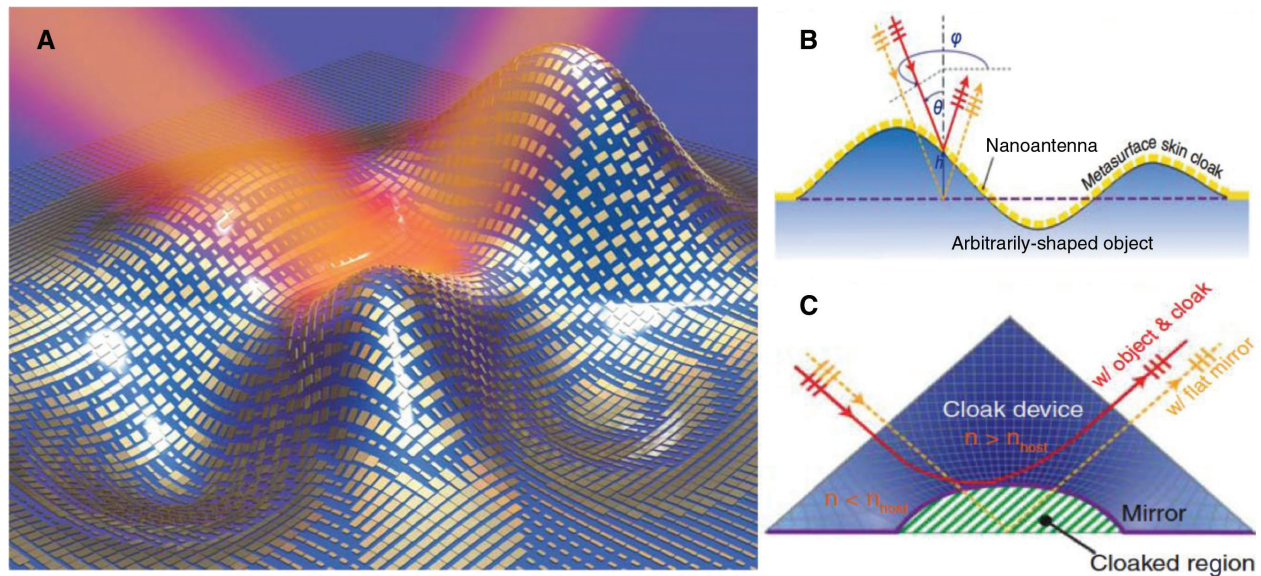
Figure 5: Schematic view and working principle of a metasurface skin cloak.
(A) The metasurface skin cloak is an ultrathin layer of nanoantennas covering an arbitrarily shaped object. (B) Working principle of the metasurface skin cloak. The metasurface fully restores the wavefront and phase of the scattered light and makes the object appear as a flat mirror. (C) Working principle of a conventional carpet cloak. The carpet cloak has spatially varying refractive index over a big volume, designed with an optical quasi-conformal mapping technique. It introduces additional phase retardation due to the light propagation inside its host material, which makes the object detectable to a phase-sensitive measuring device. Reprinted from Ref. [22]. Copyright © 2015 by the AAAS.
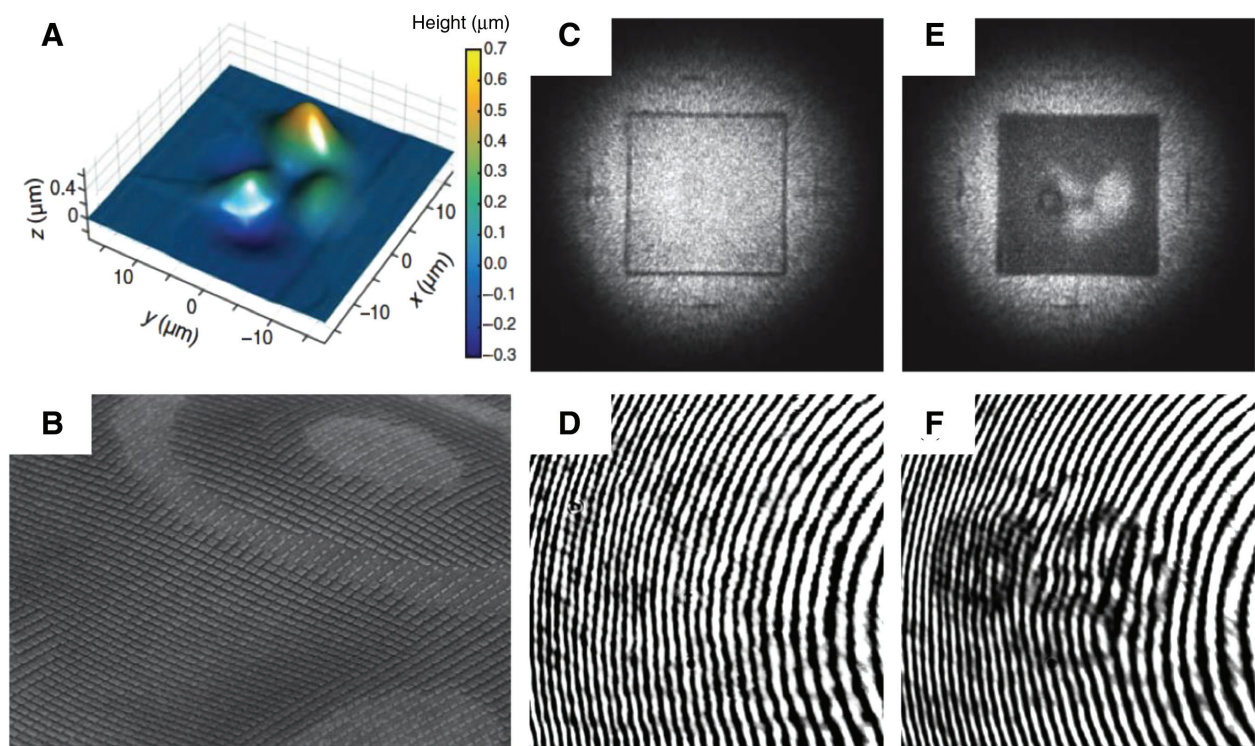

Figure 6: A metasurface invisibility skin cloak for a 3D arbitrarily shaped object.
(A) Atomic force microscopy image of a 3D arbitrarily shaped object that includes multiple bumps and dents. (B) SEM images of the object and the metasurface fabricated on top of it. (C) and (D) Reflection from the object when the cloak is on: intensity and phase measurement, respectively. The illumination laser has a wavelength of ~730 nm. (E and F) Intensity and phase measurement when the cloak is off. When the cloak is off, the object can clearly be seen in the intensity image and distorted interference fringes are shown in the phase measurement. When the cloak is on, the object appears hidden in both intensity and phase measurement. Reprinted from Ref. [22]. Copyright © 2015 by the AAAS.

was then designed and fabricated according to the height profile of the object. Experimentally, we showed that, under both direct wide-field imaging (Figure 6C and E) and phase measurement (Figure 6D and F), the metasurface cloak can successfully hide the 3D object at ~730 nm wavelength. Because the cloak is an ultrathin 2D structure, it is much easier to fabricate compared to previous volumetric cloaks and is fully scalable to macroscopic sizes.

5 Metasurface-mediated quantum interactions

Spontaneous emission is one of the most fundamental quantum phenomena in nature. In a free space (ordinary vacuum), a two-level atom in its excited state decays (via irreversible process) to the ground state at a rate [46]

$$\gamma_0 = \left(\frac{1}{4\pi\varepsilon_0}\right)\frac{4\omega_0^3\wp^2}{3\hbar c^3} \tag{1}$$

where ω_0 and $\wp$ are the atomic transition frequency and dipole moment, respectively. In his pioneering work, Purcell demonstrated that the spontaneous emission from an atom is not its intrinsic property; rather, it can be manipulated. Let us consider an atomic (electric) dipole located in the vicinity ($d \ll \lambda$) of a flat mirror, as shown in Figure 7. If the dipole is oriented parallel to the surface, its decay rate is completely suppressed; however, if the same dipole is oriented perpendicular to the surface, it exhibits an enhanced decay rate with respect to its free space value
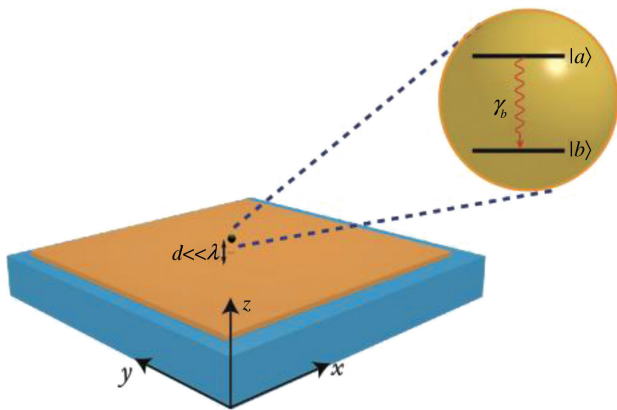

Figure 7: Dipole-mirror interface.
An atomic dipole (i.e. two-level atom with excited state |a> and ground state |b>) located in the vicinity of a mirror. Depending on the orientation of the dipole moment, the atomic dipole exhibits enhanced or suppressed emission rate.

(γ_0). Moreover, the change in the decay rate depends on the distance between the dipole and the surface and dies off at distances beyond $d \sim \lambda$. This orientation-dependent decay rate is the manifestation of anisotropic vacuum in the vicinity of the mirror. However, it is important to note that two in-plane dipoles (x-y plane) located at the same height will have same decay rates.

In 2015, we proposed and theoretically demonstrated a judiciously metasurface that can be harnessed at single photon level, which opened the door for quantum photonic applications with metasurface [23]. We showed that metasurface can be used to engineer the quantum vacuum in the vicinity of a quantum emitter located, as shown in Figure 8 (left), or trapped at a macroscopic distance from the surface and induce interference among decay channels. Recently, in 2017, we also showed that quantum correlations could be generated between two qubits located and separated by macroscopic distances, as shown in Figure 8 (right), from the metasurface [24].

It is well known that the quantum vacuum of an electromagnetic field is the key to many intriguing phenomena in quantum optics, quantum field theory, condensed matter physics, etc. In multilevel atom or atom-like systems, spontaneous emission from two (nearly) degenerate excited states to a common ground state can show interference, which has led to many counterintuitive phenomena in atomic physics [47]. The existence of such vacuum (noise)-induced quantum interference requires a stringent criterion of nonorthogonal transition dipole matrix elements corresponding to the two decay channels, which is rarely met in atomic physics. However, the anisotropy of the vacuum fluctuations can restore the quantum interference even for orthogonal dipole moments. Several schemes [48–50] for an anisotropic vacuum have been proposed and quantum interference has been studied for a quantum emitter located very close ($d \ll \lambda$) to the surface or confined geometries. Unfortunately, the minimum emitter-surface distance is often constrained by additional surface noise at submicron distances from the surface. Hence, it is critical to push the distance limitation for an anisotropic vacuum felt by the emitter.

The decay rate of an electric dipole emitter is given by [46]

$$\frac{\gamma(\mathbf{r}_0)}{\gamma_0} = 1 + \frac{6\pi\varepsilon_0}{|\mathbf{p}_1|^2}\frac{1}{k^3}\mathrm{Im}[\mathbf{p}_1^*\cdot\mathbf{E}_s(\mathbf{r}_0, \mathbf{r}_0, \omega)], \tag{2}$$

where γ_0 is the vacuum spontaneous emission decay rate, ε_0 is the vacuum permittivity, $\mathbf{p}_1 = \langle a_1 | \mathbf{r}_0 | b_1 \rangle$ is the transition dipole moment of the emitter, and $k = 2\pi/\lambda$ is the wavenumber. One can see from Eq. (2) that
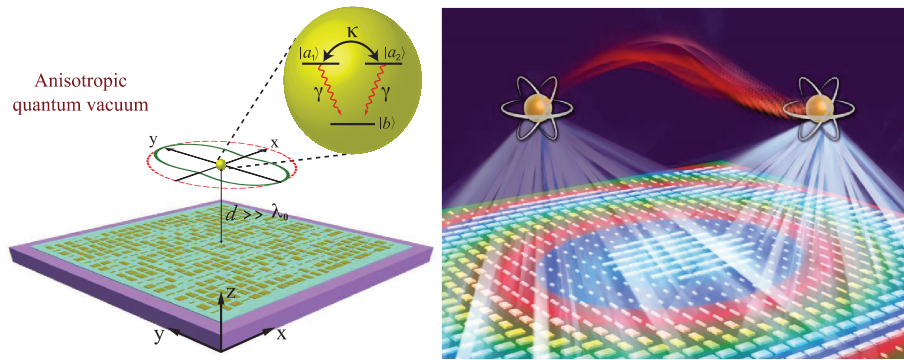
Figure 8: Metasurface-enabled quantum interference and quantum entanglement.
(Left) Multilevel quantum emitter located at a macroscopic distance from the metasurface exhibits coupling between mutually orthogonal atomic transitions. Reprinted from Ref. [23]. Copyright © 2015 by the American Physical Society. (Right) Quantum correlations between two qubits located over macroscopic distances. Using an optimally designed metasurface, emission from one qubit can be efficiently redirected toward the target qubit. Reprinted from Ref. [24]. Copyright © 2017 by the American Chemical Society.

the decay rate depends on the scattered field at the local of the emitter. One can design the metasurface such that the $Im[\mathbf{p}_1^* \cdot \mathbf{E}_s(\mathbf{r}_0, \mathbf{r}_0, \omega)] < 0$ for the x-dipole, which yields $\frac{\gamma(\mathbf{r}_0)}{\gamma_0} \sim 1$ (i.e. we suppress the decay rate). However, with the same metasurface excited by y-dipole $Im[\mathbf{p}_1^* \cdot \mathbf{E}_s(\mathbf{r}_0, \mathbf{r}_0, \omega)] \sim 0$, which yield $\frac{\gamma(\mathbf{r}_0)}{\gamma_0} \sim 1$. Such aniso-tropic response can be engineered over macroscopic distance as shown in Figure 9, where show the decay of rate of both x- and y-dipoles as a function of the distance from the metasurface. For y-dipole, we clearly see (as designed) a conventional mirror-type response; however, for x-dipole, one can suppress the decay rate over macroscopic distances. Interestingly, the upper limit to the distance for x-dipole is governed by the photonic coher-ence length. However, other factors such as fabrication defects and size of the metasurface also limit the distance d_{max}. Here, we would like to emphasize two points. First, metasurface design also gives us the flexibility to enhance

the decay rate (rather than suppressing) for an x-dipole by changing its phase profile. Second, one can also design a metasurface whose performance is vice versa (i.e. it acts a curved mirror for y-dipole while at the same time it acts as a flat mirror for x-dipole).

Anisotropic optical response yield interesting effects if we consider a multilevel (in particular three-level atom) quantum emitter as shown in Figure 9 (right). To study the effect of anisotropic quantum vacuum on the dynam-ics of a three-level atom with mutually orthogonal transi-tion, we started with an atom in the excited state $|a_1\rangle$ and located at the focal spot of the metasurface (acting as a curved mirror). In free space, the population of the level $|a_1\rangle$ will follow exponential decay (linear on the log-scale) as shown by the dashed green curve. However, in the pres-ence of the metasurface, the transitions $|a_{1,2}\rangle \to |b\rangle$ are coupled and the decay of the level $|a_1\rangle$ is slowed down (dashed red curve). More interestingly, we have a finite population transferred to the level $|a_2\rangle$ (solid red curve). Such radiative excitation of the orthogonal states is "only"
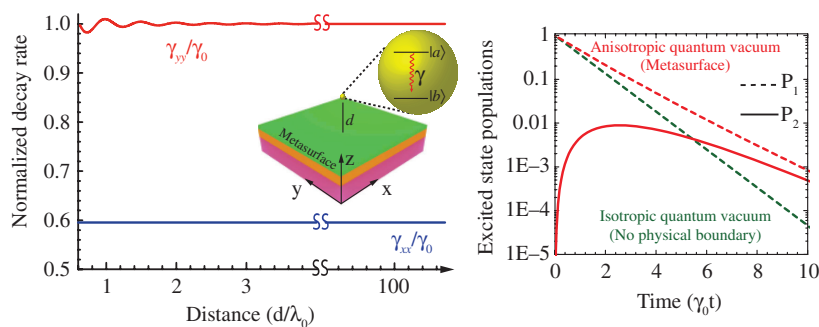

Figure 9: Metasurface-enabled in-plane anisotropic decay rate and population-coherence coupling.
(Left) Decay rate of x-dipole (blue curve) and y-dipole (red curve) against the distance from the metasurface and (right) Plot of the population of the level $|a_{1,2}\rangle$ in the presence (red curves) and absence (green curve) of the metasurface. Reprinted from Ref. [23]. Copyright © 2015 by the American Physical Society.

possible in the presence of the metasurface. Furthermore, controlling the interaction between the atomic and molecular excitation channels has led to several interesting effects [51–55].

In 2017, we proposed and theoretically demonstrated that an optimally designed metasurface can be used to generate quantum correlation between two qubits by introducing interaction channels mediated by the metasurface. Figure 10 (left) shows the transient evolution of concurrence between two qubits located at $h = 10\lambda$ from the metasurface and separated by a distance of $d = 20\lambda$ and initially prepared in the separable state $|\Psi_{12}(0)\rangle = |a_1\rangle \otimes |b_2\rangle$. In the presence of the metasurface (blue line), the maximum value of concurrence is 0.366, which is two orders of magnitude higher than vacuum (red line). The heat map in the inset shows the maximum value of concurrence in the collective parameters space. Green and black lines denote equal maximum concurrence lines of lossless and actual metasurfaces, respectively.

Common approaches to entangle qubits use, *inter alia*, waveguides [56], localized surface plasmon [57], photonic crystals [58], and microcavities [59]. Efficient entanglement via these platforms requires stringent near-field position of the qubits, which is imperative for achieving high β factor. However, this requirement is an arduous task in experiments. Moreover, plasmonic waveguides lack scalability to macroscopic distances due to ohmic losses. In light of these inherent limitations of the existing platforms to enable on-chip quantum entanglement of macroscopically separated qubits, which are trapped in the far field, the metasurface scheme offers an appealing platform with novel and unconventional results. As for the metasurface case, the qubits are in the far field (located at a height of 20λ above the metasurface), whereas for the plasmonic waveguide case the qubits are in the near field; the metasurface platform provides a route for a more feasible experimental demonstration, as it is immune to the stringent plasmonic near-field position requirement of the qubits. We would like to highlight that, in the scheme of our metasurface, the interaction channel between the qubits is a far-field channel; thus, they offer an opportunity for a spatially scalable architecture to entangle qubits. By spatially scalable, we refer to the ability of the metasurface to efficiently redirect the light from the source qubit to the target qubit for any given separation between them. Such a unique capability results in the dependence of the phase profile imparted by the metasurface on the separation between the qubits. Figure 10 (right) shows the maximum concurrence between two qubits as a function of distance. We see that, in the near-field regime ($d \ll \lambda$), the entanglement achieved in the presence of metasurface coincides with qubits in vacuum, however, as the separation between the qubits increases, beyond wavelength, we clearly see the advantage of the metasurface.

There are several opportunities to experimentally verify metasurface-mediated far-field anisotropic quantum vacuum and entangled qubits. We begin with our first choice, which is trapped atoms. In stark contrast to the solid-state quantum emitters, atoms benefit from being identical with well-known atomic transitions in optical regime, easily polarizable, and their optical properties can be controlled on ultrafast time scales. The cooling and trapping of single atoms (alkali atoms) are done very routinely in a cold atom community [60]. More importantly, the precision in the location of the trapped atom could be within tens of nanometers from the desired position. On the contrary, solid-state quantum emitters such as quantum dots, color-centers, and defects in 2D
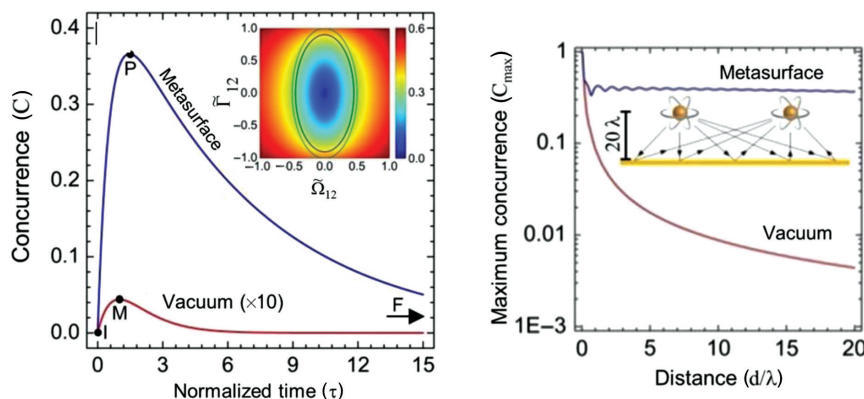

Figure 10: Metasurface-mediated quantum entanglement between two distant qubits.
(Left) Plot of concurrence between two qubits as a function of time and (right) plot of maximum concurrence against the distance between the qubits. Reprinted from Ref. [24]. Copyright © 2018 by the American Chemical Society.

semiconductors could also serve as a two-level system. The key requirements for selecting quantum emitters (atomic or solid-state) are (a) in-plane dipole moment and (b) good quantum yield. The first requirement stems from metasurface nanoantennas, which only respond to electric field parallel to the antennas. On the contrary, high quantum yield is required for measurable signal-to-noise ratio. Whereas atoms need to be cooled down to micro-nano Kelvin, solid-state emitters work well at a temperature of ~4 K. Recently, defects in hexagonal boron nitride has shown good quantum yield with narrower linewidth at room temperature [61] and quantum emission from these defects has emerged as a new candidate for solid-state quantum optics. Engineering the quantum vacuum could enable a quantum process that is forbidden in free space and open new opportunities at single photon level with application from fundamental physics to quantum technologies.

6 Conclusion and perspective

In the recent years, metasurface research has grown tremendously from experiments demonstrating rich physics to enormous potentials for technological advancements. We have demonstrated an invisibility cloak for visible light that is only a few tens of nanometers thick. The ultrathin skin cloak is fully scalable and has no size limitations. We expect that, with the development of large-scale nanofabrication, macroscopic metasurface skin cloak will 1 day come to practice. In addition to application achievement, we are also interested in developing new design principles of metasurfaces beyond the phase gradient regime. Instead of assuming negligible interactions between meta-atoms, we have shown that the coupling can be used to manipulate light at the deep subwavelength scale. Observed phenomena such as enhanced quality factor and reduced detrimental crosstalk could be very useful when designing metasurface with very small pixel size and closely spaced resonators. Moreover, we are interested in using metasurfaces to study the fundamental properties of light or light-matter interactions. By fabricating a metasurface with rapid phase gradient, we have demonstrated strong PSHE, which is otherwise hard to observe in nature. Metasurfaces can also be applied in quantum physics studies. Using metasurfaces to engineer vacuum properties at the far field, we theoretical showed that strong quantum interference could be induced in a three-level atom. Due to the their great design flexibility

and thin planar structure, metasurfaces can be a promising candidate for on-chip quantum studies.

References

[1] Pendry JB, Holden AJ, Stewart WJ, Youngs II. Extremely low frequency plasmons in metallic mesostructures. Phys Rev Lett 1996;76:4773–6.

[2] Pendry JB, Holden AJ, Robbins DJ, Stewart WJ. Magnetism from conductors and enhanced nonlinear phenomena. IEEE Trans Microw Theory Techn 1999;47:2075–84.

[3] Veselago VG. The electrodynamics of substances with simultaneously negative values of ε and μ. Sov Phys Uspekhi 1968;10:509–14.

[4] Pendry JB. Negative refraction makes a perfect lens. Phys Rev Lett 2000;85:3966–9.

[5] Fang N, Lee H, Sun C, Zhang X. Sub-diffraction-limited optical imaging with a silver superlens. Science 2005;308:534–7.

[6] Schurig D, Mock JJ, Justice BJ, et al. Metamaterial electromagnetic cloak at microwave frequencies. Science 2006;314:977–80.

[7] Holloway CL, Kuester EF, Gordon JA, O'Hara J, Booth J, SmithDR. An overview of the theory and applications of metasurfaces: the two-dimensional equivalents of metamaterials. IEEE Antennas Propag Mag 2012;54:10–35.

[8] Kildishev AV, Boltasseva A, Shalaev VM. Planar photonics with metasurface. Science 2013;339:1232009.

[9] Yu N, Genevet P, Aieta F, et al. Flat optics: controlling wavefronts with optical antenna metasurfaces. IEEE J Sel Top Quant Electron 2013;19:4700423.

[10] Yu N, Capasso F. Flat optics with designer metasurfaces. Nat Mater 2014;13:139.

[11] Yu N, Genevet P, Kats MA, et al. Light propagation with phase discontinuities: generalized laws of reflection and refraction. Science 2011;334:333–7.

[12] Ni X, Emani NK, Kildishev AV, Boltasseva A, Shalaev VM. Broadband light bending with plasmonic nanoantennas. Science 2012;335:427.

[13] Pors A, Albrektsen O, Radko IP, Bozhevolnyi SI. Gap plasmon-based metasurfaces for total control of reflected light. Sci Rep 2013;3:2155.

[14] Hasman E, Kleiner V, Biener G, Niv A. Polarization dependent focusing lens by use of quantized Pancharatnam-Berry phase diffractive optics. Appl Phys Lett 2003;82:328–30.

[15] Decker M, Staude I, Falkner M, et al. High-efficiency dielectric Huygens' surfaces. Adv Opt Mater 2015;3:813–20.

[16] Khorasaninejad M, Chen WT, Devlin RC, Oh J, Zhu AY, Capasso F. Metalenses at visible wavelengths: diffraction-

limited focusing and subwavelength resolution imaging. Science 2016;352:1190–4.

[17] Lin D, Fan P, Hasman E, Brongersma ML. Dielectric gradient metasurface optical elements. Science 2014;345:298–302.

[18] Ni X, Kildishev AV, Shalaev VM. Metasurface holograms for visible light. Nat Commun 2013;4:2807.

[19] Zheng G, Mühlenbernd H, Kenney M, Li G, Zentgraf T, Zhang S. Metasurface holograms reaching 80% efficiency. Nat Nano 2015;10:308–12.

[20] Maguid E, Yulevich I, Veksler D, Kleiner V, Brongersma ML, Hasman E. Photonic spin-controlled multifunctional shared-aperture antenna array. Science 2016;352:1202–6.

[21] Yin X, Ye Z, Rho J, Wang Y, Zhang X. Photonic spin Hall effect at metasurfaces. Science 2013;339:1405–7.

[22] Ni X, Wong ZJ, Mrejen M, Wang Y, Zhang X. An ultrathin invisibility skin cloak for visible light. Science 2015;349:1310–4.

[23] Jha PK, Ni X, Wu C, Wang Y, Zhang X. Metasurface-enabled remote quantum interference. Phys Rev Lett 2015;115:025501.

[24] Jha PK, Shitrit N, Kim J, Ren X, Wang Y, Zhang X. Metasurface-mediated quantum entanglement. ACS Photon 2018;5:971–6.

[25] Zhang S, Ye Z, Wang Y, et al. Anti-Hermitian plasmon coupling of an array of gold thin-film antennas for controlling light at the nanoscale. Phys Rev Lett 2012;109:193902.

[26] Okolowicz J, Ploszajczak M, Rotter I. Dynamics of quantum systems embedded in a continuum. Phys Rep 2003;374:271–383.

[27] Liu N, Langguth L, Weiss T, et al. Plasmonic analogue of electromagnetically induced transparency at the Drude damping limit. Nat Mater 2009;8:758–62.

[28] Zhang S, Genov DA, Wang Y, Liu M, Zhang X. Plasmon-induced transparency in metamaterials. Phys Rev Lett 2008;101:047401.

[29] Jha PK, Mrejen M, Kim J, et al. Interacting dark resonances with plasmonic meta-molecules. Appl Phys Lett 2014;105:111109.

[30] Zelevinsky V. Quantum physics volume 1: from basics to symmetries and perturbations. Weinheim, Wiley-VCH; Verlag GmbH & Co. KGaA, 2011, 551.

[31] Soshin C, Graham CD. Physics of ferromagnetism. 2nd ed. Vol. 94. Oxford, UK, Oxford University Press on Demand, 2009.

[32] Bernevig BA, Yu X, Zhang SC. Maxwell equation for coupled spin-charge wave propagation. Phys Rev Lett 2005;95:076602.

[33] Gorodetski Y, Bliokh KY, Stein B, et al. Weak measurements of light chirality with a plasmonic slit. Phys Rev Lett 2012;109:013901.

[34] Alù A. Mantle cloak: Invisibility induced by a surface. Phys Rev B 2009;80:245115.

[35] Fan P, Chettiar UK, Cao L, Afshinmanesh F, Engheta N, Brongersma ML. An invisible metal-semiconductor photodetector. Nat Photon 2012;6:380–5.

[36] Pendry JB, Schurig D, Smith DR. Controlling electromagnetic fields. Science 2006;312:1780–2.

[37] Leonhardt U. Optical conformal mapping. Science 2006;312:1777–80.

[38] Sanchis L, García-Chocano VM, Llopis-Pontiveros R, et al. Three-dimensional axisymmetric cloak based on the cancellation of acoustic scattering from a sphere. Phys Rev Lett 2013;110:124301.

[39] Zhang S, Genov DA, Sun C, Zhang X. Cloaking of matter waves. Phys Rev Lett 2008;100:123002.

[40] Li J, Pendry JB. Hiding under the carpet: a new strategy for cloaking. Phys Rev Lett 2008;101:203901.

[41] Liu R, Ji C, Mock JJ, Chin JY, Cui TJ, Smith DR. Broadband ground-plane cloak. Science 2009;323:366–9.

[42] Gharghi M, Gladden C, Zentgraf T, et al. A carpet cloak for visible light. Nano Lett 2011;11:2825–8.

[43] Hsu LY, Lepetit T, Kante B. Extremely thin dielectric metasurface for carpet cloaking. Prog Electromagn Res 2015;152:33–40.

[44] Orazbayev B, Estakhri NM, Alù A, Beruete M. Experimental demonstration of metasurface-based ultrathin carpet cloak for millimetre waves. Adv Opt Mater 2016;5:1600606.

[45] Estakhri NM, Alù A. Ultra-thin unidirectional carpet cloak and wavefront reconstruction with graded metasurfaces. IEEE Antennas Wireless Propag Lett Spec Cluster Transform Electromagn 2014;13:1775–8.

[46] Novotny L, Hecht B. Principles of nano-optics. Cambridge, England: Cambridge University Press, 2006.

[47] Agarwal GS. Quantum statistical theories of spontaneous emission and their relation to other approaches. In: Hohler G., ed. Springer tracts in modern physics: quantum optics. Vol. 70, Berlin: Springer-Verlag, 1974.

[48] Agarwal GS. Anisotropic vacuum-induced interference in decay channels. Phys Rev Lett 2000;84:5500–3.

[49] Vassilios Y, Paspalakis E, Vitanov NV. Plasmon-induced enhancement of quantum interference near metallic nanostructures. Phys Rev Lett 2009;103:063602.

[50] Li G, Li F, Zhu S. Quantum interference between decay channels of a three-level atom in a multilayer dielectric medium. Phys Rev A 2001;64:013819.

[51] Jha, PK. Using quantum coherence to enhance gain in atomic physics. Coherent Opt Phenom 2013;1:25–41.

[52] Jha PK, Mrejen M, Kim J, et al. Coherence-driven topological transition in quantum metamaterials. Phys Rev Lett 2016;116:165502.

[53] Ramezani H, Jha PK, Wang Y, Zhang X. Nonreciprocal localization of photons. Phys Rev Lett 2018;120:043901.

[54] Tsakmakidis KL, Jha PK, Wang Y, Zhang X. Quantum coherence-driven self-organized criticality and nonequilibrium light localization. Sci Adv 2018;4:eaaq0465.

[55] Dorfman KE, Jha PK, Voronine DV, Genevet P, Capasso F, Scully MO. Quantum-coherence-enhanced surface plasmon emission by stimulated emission of radiation. Phys Rev Lett 2013;111:043601.

[56] Gonzalez-Tudela A, Martin-Cano D, Moreno E, Martin-Moreno L, Tejedor C, Garcia-Vidal FJ. Entanglement of two qubits mediated by one-dimensional plasmonic waveguides. Phys Rev Lett 2011;106:020501.

[57] Nerkararyan KV, Bozhevolnyi SI. Entanglement of two qubits mediated by a localized surface plasmon. Phys Rev B 2015;92:045410.

[58] Goban, A, Hung C-L, Hood JD, et al. Superradiance for atoms trapped along a photonic crystal waveguide. Phys Rev Lett 2015;115:063601.

[59] Hagley E, Maître X, Nogues G, et al. Generation of Einstein-Podolsky-Rosen pairs of atoms. Phys Rev Lett 1997;79:1–5.

[60] Bloch I. Ultracold quantum gases in optical lattices. Nat Phys 2005;1:23–30.

[61] Tran TT, Bray K, Ford MJ, Toth M, Aharonovich I. Quantum emission from hexagonal boron nitride monolayers. Nat Nano 2016;11:37–41.